Biosensors and Bioelectronics xxx (2010) xxx–xxx

Contents lists available at ScienceDirect

Biosensors and Bioelectronics

journal homepage: www.elsevier.com/locate/bios

LED-based Interferometric Reflectance Imaging Sensor for quantitative dynamic monitoring of biomolecular interactions

G.G. Daaboul[a], R.S. Vedula[a], S. Ahn[a], C.A. Lopez[b], A. Reddington[b], E. Ozkumur[b], M.S. Ünlü[a,b,c,*]

[a] Dept. of Biomedical Engineering, Boston University, 44 Cummington St., Boston, MA 02215, USA
[b] Dept. of Electrical and Computer Engineering, Boston University, 8 St. Mary's St., Boston, MA 02215, USA
[c] Physics Dept., Boston University, 590 Commonwealth Ave., Boston, MA 02215, USA

ARTICLE INFO

Article history:
Received 25 June 2010
Received in revised form
11 September 2010
Accepted 21 September 2010
Available online xxx

Keywords:
Interferometry
Label-free
Biosensor
High-throughput assay
DNA/protein microarray
Imaging
LED

ABSTRACT

Label-free optical biosensors have been established as proven tools for monitoring specific biomolecular interactions. However, compact and robust embodiments of such instruments have yet to be introduced in order to provide sensitive, quantitative, and high-throughput biosensing for low-cost research and clinical applications. Here we present the Interferometric Reflectance Imaging Sensor (IRIS) using an inexpensive and durable multi-color LED illumination source to monitor protein–protein and DNA–DNA interactions. We demonstrate the capability of this system to dynamically monitor antigen–antibody interactions with a noise floor of 5.2 pg/mm^2 and DNA single mismatch detection under denaturing conditions in an array format. Our experiments show that this platform has comparable sensitivity to high-end label-free biosensors at a much lower cost with the capability to be translated to field-deployable applications.

1. Introduction

Development of label-free biosensors that can simultaneously monitor multiple molecular interactions is of great interest for biomedical research and clinical applications (Stears et al., 2003; MacBeath and Schreiber, 2000; Predki, 2004; Zhu et al., 2001). The importance of detecting interactions between DNA–DNA, DNA–protein, and antibody–antigen pairs have been firmly established by the ubiquity of ELISA and fluorescent microarray techniques (Mitchell, 2002; Yu et al., 2006). Though label-based immunoassay and microarray methods are very powerful, there is significant interest in developing label-free detection modalities that can improve upon the limitations of these systems. Generally, label-free detection has been demonstrated with electrical, electromechanical, and optical detection methods (Andras et al., 2009; Ramachandran et al., 2005; Ramsden, 1997; Winquist et al., 1997). Among optical platforms, Surface Plasmon Resonance (SPR) has proven to be the leading technology and through utilization of SPR imaging (SPRi), high-throughput detection has been achieved (Homola et al., 2005). Though SPRi is a very powerful technique, the progression of this technology is moving toward simplicity, inexpensive device and operation costs, and field use.

Another category of optical platforms that has received significant attention in recent years and may be suitable for such applications is based on new adaptations of reflectance spectroscopy. Traditionally a single-point measurement, reflection spectroscopy has relied on a broadband light source for surface illumination and a spectrometer for analysis of the reflected light. In this approach, surface reflections are characterized for alterations (ex: changes in polarization state or phase modulation) to derive information about properties of the reflecting surface such as thickness or refractive index. Spectroscopic ellipsometry, a technique that has been utilized for nearly a century to interrogate thin dielectric films, is a well known example of detection methods in this category. Many recent innovations of interferometric spectroscopy have been applied to biodetection demonstrating the diverse and versatile nature of this methodology. For example, Arrayed Imaging Reflectometry (AIR), a system based on reflectance measurements, works by illuminating a planar layered structure with a specific wavelength of light and incident angle to produce complete destructive interference. Bioaccumulation results in an increase in the reflectivity whereby the Fresnel equation can be used to determine the amount of material bound (Lu et al., 2004). Another technique, termed Molecular Interferometric Imaging (MI2) relies on using a reference signal which is restricted to

* Corresponding author at: College of Engineering, 8 St. Mary's Street, Boston, MA 02215, USA. Tel.: +1 617 353 5067; fax: +1 617 353 6440.
E-mail address: selim@bu.edu (M.S. Ünlü).

0956-5663/$ – see front matter © 2010 Elsevier B.V. All rights reserved.
doi:10.1016/j.bios.2010.09.038

phase quadrature to determine bioaccumulation (through commonly known phase and intensity relationships). By keeping a reference light phase-locked to quadrature the change in reflected amplitude of the light is maximized thus allowing for sensitive detection (Zhao et al., 2008). A third approach, Reflectometric Interference Spectroscopy (RIfS) employs white light-based interference patterns produced by transparent substrates with thicknesses of several micrometers. To determine binding, this technique monitors the shift in one maximum of the interference pattern, and has system resolution values of optical thickness of less than 1 pm (Lange et al., 2004).

Recently, we have introduced a simple reflectance-based interferometric label-free detection method originally termed the Spectral Reflectance Imaging Biosensor (SRIB) and recently renamed as the Interferometric Reflectance Imaging Sensor (IRIS) that has demonstrated comparable sensitivity to SPR (Ozkumur et al., 2008). To detect molecular interactions, this technique uses common-path interferometry through a Si/SiO_2 layered substrate acting as the sensor surface by monitoring local optical path length changes attributed to mass accumulation at the surface. IRIS has proven to be a versatile platform to monitor antigen–antibody binding, DNA hybridization, and single nucleotide polymorphisms (SNPs) through DNA denaturation kinetics (Özkumur et al., 2010; Ozkumur et al., 2008, 2009). The IRIS platform relied on a tunable laser source to monitor the spectral signature of the reflection from the layered sensor surface in an imaging modality. However tunable lasers are both expensive and delicate, limiting the applications in field-deployable systems. Moreover, the use of the coherent laser source can result in image artifacts due to interference of light reflected and scattered from various components in the optical path.

In this article, we introduce a second generation of the IRIS platform described above, that addresses the drawbacks of the original system by utilizing multiple discrete LED sources to monitor the spectral signature of reflectance from the layered biosensor surface. This new system can achieve the same level of system sensitivity and measurement confidence by employing only a few incoherent, narrow band sources that span the visual spectrum. It is demonstrated that this new LED-based IRIS system can monitor biological binding interactions in a real-time, high-throughput microarray format with a 5.2 pg/mm^2 noise floor. The system offers ease-of-use in a compact, low-power, and stable design making it a robust solution that can translate the performance of more complex and expensive label-free platforms such as SPRi and Laser-IRIS, to a broad spectrum of research and diagnostic applications both in the clinic and field.

2. Materials and methods

2.1. LED-IRIS method of detection

Interferometric techniques are widely used to measure minute differences in optical path lengths. In a biosensing modality, these measured optical path length differences can be due to the capture of a target of interest. Layered substrates demonstrate characteristic spectral reflectance due to the interference of reflected light form the layer interfaces, in this case, the $Si–SiO_2$ interface and the SiO_2–air interface. A change in optical path length difference due to added biomass on the oxide layer causes a quantifiable shift in this wavelength-dependent reflectivity curve. The three black curves shown in Fig. 1a illustrate how the spectral reflectivity of the bi-layered substrate starting at 500 nm of oxide shifts due biomass accumulation, illustrated here as 5 nm incremental increases in thickness.

The principle of detection for the LED-IRIS is based on quantifying these shifts in the spectral reflectance signature to calculate the added biomass by sampling it at specific wavelengths and measuring the characteristic reflection intensities using a CCD camera (Fig. 1b) (optical schematic Figure 1S). The sensor surface is sequentially illuminated using an ACULED VHL surface-mount LED package (Perkin-Elmer), which has four independently driven LEDs with peak emission wavelengths of 455 nm, 518 nm, 598 nm, and 635 nm. Fig. 1a demonstrates the sampling of the reflectivity curve with these four LEDs where the spectral bandwidths of the LEDs are represented by the Gaussian functions. The position of the LEDs' emission spectra with respect to the reflectance curve is critical for allowing the accurate measurement of the shift due to a change in the thickness of the top layer. The spectra of three of the LEDs (455 nm, 518 nm, and 635 nm) were chosen to sample the linear region of the reflectance curve. The near symmetry of the LEDs' emission spectra when sampling the linear region of the curve allows for approximating the LED emission as a single peak at the central wavelength. The yellow LED (598 nm) helps the fitting by pinning the minimum of the reflectance curve over one period.

After acquiring images of the substrate for each of the four wavelengths each pixel of the CCD represents an individual measurement of the reflective interference intensity of light at each wavelength, forming a three-dimensional array of data (pixel, wavelength, intensity) for the entire sensor. The data points for each pixel are fitted to a curve derived using well know formulations, which governs the behavior of reflection from a semi-transparent bi-layered substrate (Ozkumur et al., 2008; Yeh, 1988). To achieve

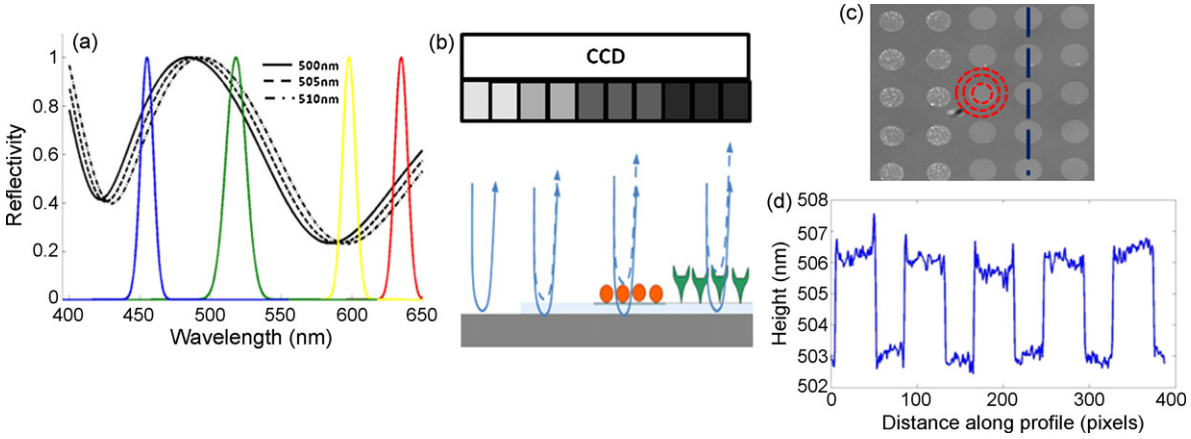

Fig. 1. Method of detection: (a) displays the shift of the reflectivity curve due to 5 nm step increases in thickness on the surface. The colored Gaussians represent the 4 LEDs used to sample the curve. (b) Schematic of the sensor's imaging path illustrating biomass accumulation dependent grayscale intensity changes. (c) Example of the sensor's surface with an array of protein spots. (d) Height profile along the dashed line in (c) across spots.

Please cite this article in press as: Daaboul, G.G., et al., Biosens. Bioelectron. (2010), doi:10.1016/j.bios.2010.09.038

repeatable measurements the intensity of the incident light must be know. Incident light is traditionally monitored by using an external photodetector; however, to maintain the simplicity of the system an on-chip reference is utilized. The reference region is created by etching a bare silicon region on the substrate that is placed in the field of view to normalize for any fluctuations in the incident light intensity (Vedula et al., 2010). After fitting every pixel in the image, the surface topography of the sensor's surface is presented in a grayscale image where brighter regions indicate greater thickness on the surface (Fig. 1c). The height profile across the 5 protein spots along the dashed line are shown in Fig. 1d. To determine spot height the average height from pixels in an annular region outside of the spot (background) is subtracted from the average height of pixels inside a spot (Fig. 1c).

2.1.1. Surface functionalization

The interferometric measurements were made on 15 mm square silicon chips with 500 nm of thermally grown oxide purchased from Silicon Valley Microlelectronics (Santa Clara, CA). The samples were sonicated and washed extensively using acetone, methanol, and deionized water to remove any dust and impurities. To functionalize the surface for immobilization of biomolecules, the chips were coated with a copoly(N,N-dimethylacrylamide (DMA)–acryloyloxysuccinimide (NAS)–3(trimethoxysilyl)-propyl methacrylate (MAPS)) polymer described in detail elsewhere (Cretich et al., 2004). Briefly, the samples were first washed in a solution of .1 M NaOH to activate the surface for polymer coating. Then the chips were immersed in the polymer solution (1%, w/v polymer in an aqueous solution of 20% saturated ammonium sulfate) for 30 min, then washed extensively with DI water, dried with argon, and baked at 80 °C for 15 min. The polymer-coated chips were kept in a dessicator until use. The polymer coating covalently attaches to the oxide surface and is used to immobilize biological probes using N-hydroxysuccinimide chemistry via amide linkages.

2.1.2. BSA spotting for quantification and calibration

The response of the system to a given adsorbed mass on the surface was quantified using purified bovine serum albumin (BSA) (Sigma, St. Louis, MO). The purification and precise spotting of BSA on the sensor's surface was described in detail in (Ozkumur et al., 2009). Briefly, after BSA was purified through dialysis it was lyophilized and re-dissolved in milli-Q water to a concentration of 2 mg/ml. Then the BSA was serially diluted in milli-Q water using high precision pipettes from Gilson (Middleton, WI). The solutions were spotted using a Scienion SciFlexarrayer S5 piezoelectric arrayer (Berlin, Germany) equipped with the sciDropVOLUME software, a tool to measure the absolute volume of the droplets dispensed by a SciFlexarrayer piezo nozzle. For each spot, a photograph of the actual droplet in mid air is used to calculate the spotted volume. Based on the spot volume and concentration of the BSA solution, BSA was spotted from 25 pg to 400 pg. IRIS measurements were made on the sensor's surface after water was allowed to evaporate leaving behind only the protein on the surface.

2.1.3. Array preparation and dynamic binding measurement

Biomolecules were spotted with BioOdyssey Caligrapher MiniArrayer (Bio-Rad) after surface functionalization. Human serum albumin (HSA), rabbit IgG (RA), anti-rabbit IgG (α-RA) and mouse IgG (MA) were purchased from Sigma (St. Louis, MO); anti-HSA (α-HSA) was purchased from Abcam (Cambridge, MA). All proteins were spotted at 1 mg/mL concentration in PBS (pH 7.4). All DNA oligonucleotides were purchased from Integrated DNA Technologies (Coralville, IA). The sequence of the probes are shown in Table 1S, and the design criteria for the probes are described elsewhere (Özkumur et al., 2010). All oligonucleotide probes were 5′ amine functionalized for immobilization on the polymer surface. Spotting concentration was 25 μM in 150 mM sodium phosphate buffer (pH 8.5).

The spotted arrays were kept overnight at 75% humidity to allow the probes to bind to the surface and inactivate any unbound NHS groups to prevent later background binding. The protein arrays were washed 3 times in 1× PBS with 0.2% Tween, 3 times in 1× PBS, and 3 times in DI water for 30 s each on a shaker and then dried with argon gas. The DNA arrays were washed 4 times in 6× SSPE with 0.01% Tween on a shaker for 10 min each, rinsed with DI water, and dried with argon gas.

Samples were placed in a custom made flow cell with a volume of 120 μL to measure real-time biomolecular interactions. Target analyte solutions were filtered (0.22 um, Millipore) prior to the experiment to remove impurities. The flow was driven by a peristaltic pump (Control Company, Friendswood, TX) at a constant flow rate of 120 uL/min. The flow chamber was sealed by a silicone rubber sheet and glass window with an anti-reflection coating in the visible and near IR range (Edmund Optics). Incubations and measurements took place at room temperature. The same five proteins that were used for spotting were used as targets to study protein–protein interaction. HSA, α-HSA, RA, α-RA, and MA were flowed in sequentially at a concentration of 1 μg/mL in PBS. For DNA interaction studies, both target oligonucleotides were flowed in at a concentration of 1 μM in a hybridization buffer that was composed of 100 mM MES, 1 M [Na^+], and 20 mM EDTA buffer. The hybridization buffer was diluted 1:20 and used as the wash buffer following hybridization. It was further diluted to have 0.5 mM [Na^+] in order to monitor denaturation kinetics of a single nucleotide mismatch hybrids.

3. Results and discussion

3.1. Quantification and calibration

Fig. 2a shows the BSA spotted sample used for calibration of measured optical path length difference due to accumulated biomass. As outlined in the methods section, the spotted mass was calculated from the spot volume and concentration of the BSA solution. The average IRIS measurements (spot height) of a 3 × 6 array for each of the spotted conditions, normalized by the spot area, is plotted versus the spotted mass, demonstrating a linear fit with an $R^2 = 0.99$ (Fig. 2b). From the slope of the linear fit a relationship between the surface density of the spotted BSA and measured height was calculated to be 1.3 ng/mm^2 for 1 nm of height increase. This calibration differs from the value established by Özkumur by 8%, a difference which can be attributed to experimental differences such as inaccuracies in the preparation of the known protein solutions used for spotting (Özkumur et al., 2010). In a previous experiment the noise floor of the instrument was measured on a dry sample with BSA spots to be 4 pm, which corresponds to a density of 5.2 pg/mm^2 (Figure 2S). The noise floor is defined as the RMS around the mean of the height measurement of the same protein spots over 20 independent measurements spanning approximately 30 min. The spotted BSA density for 400 pg of total mass was calculated to be approximately 10 ng/mm^2. Therefore the linearity of the data shows that this system can accurately measure surface mass from 5.2 pg/mm^2 to 10 ng/mm^2, a dynamic range of four orders of magnitude. This experiment demonstrates that four LEDs can achieve the same quantification power and system linearity for IRIS measurements as a tunable laser which uses a narrow (1 nm) bandwidth to sample the reflectivity curve.

Please cite this article in press as: Daaboul, G.G., et al., Biosens. Bioelectron. (2010), doi:10.1016/j.bios.2010.09.038

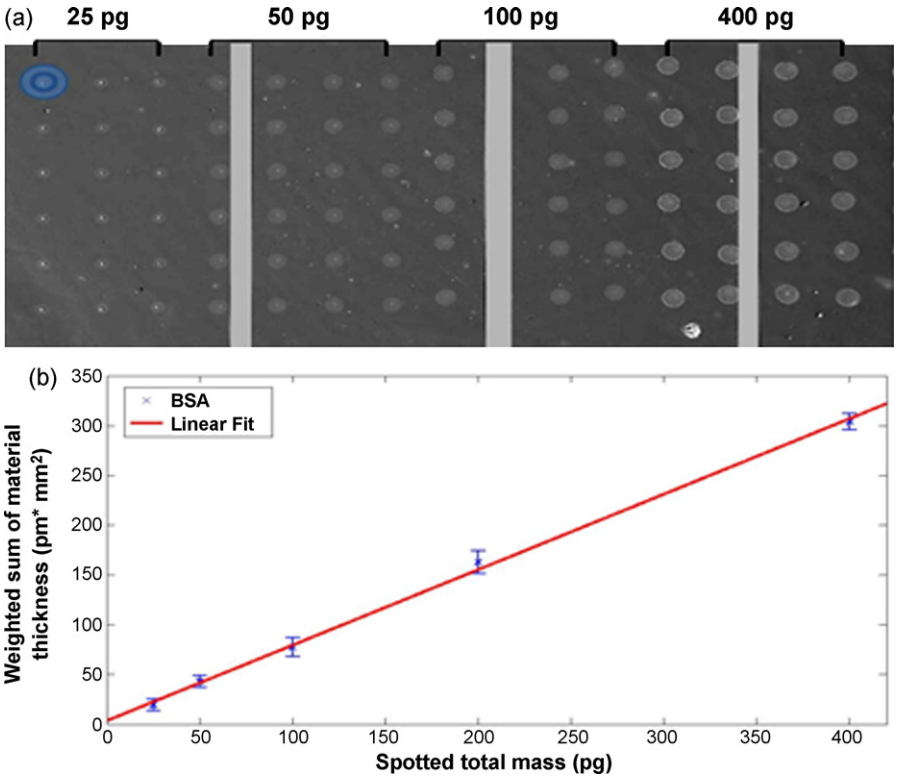

Fig. 2. Quantification and Calibration: (a) Fitted grayscale LED-IRIS image of BSA spotted at different masses. (b) Plot of weighted sum of material thickness from LED-IRIS measurements versus spotted mass on the surface. The *y*-axis is given as nm mm^2 by multiplying the average spot height by the area of the inner circle to normalize for varying spot sizes. The error bars reflect the standard deviation for 16 spots of the same condition.

3.2. Dynamic measurement of protein–protein binding

The LED-IRIS is capable of multiplexed detection of multiple target–probe interactions on the same functionalized sample. To demonstrate the multiplexed detection capability of the platform for monitoring dynamic protein–protein interactions, five spotted antigens and antibodies were monitored (HSA, anti-HSA (α-HSA), rabbit IgG (RA), anti-rabbit IgG (α-RA), mouse IgG (MA)) as their complementary targets were flowed in Fig. 3a–e show grayscale images taken after the flow of each complementary target demonstrating the incremental height change of the spotted conditions. Measurements were taken every 2 min to monitor binding kinetics of the introduced target to its corresponding probe on the surface (Fig. 3b). Initially, PBS was flowed for 15 min to wash off any non-covalently bound probes. The PBS wash cycle was repeated after the introduction of a new target into the flow chamber. After the PBS wash, HSA was introduced into the flow chamber for 50 min and 0.3 ng/mm^2 of binding was detected on the α-HSA spot. Then

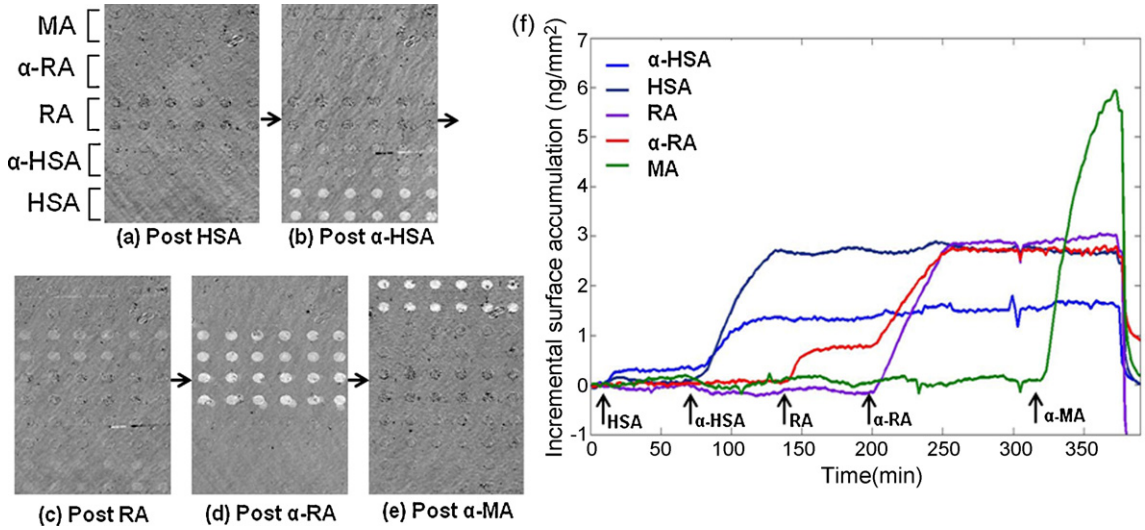

Fig. 3. Dynamic protein binding interactions: (a) series of IRIS images showing incremental height change for 12 spots each of 5 different probes on the sensor's surface. (b) Plot showing the dynamic binding kinetics of the different antigen–antibody pairs. The kinetics of a single spot is shown for each of the conditions with an RMS noise floor of 20 pm per spot calculated during the initial PBS wash. Time points at which specific targets were introduced into the flow chamber are specified. The drop at the end of the experiment is caused by the flow of 20 mM hydrochloric acid to regenerate the sensor surface for reuse.

Please cite this article in press as: Daaboul, G.G., et al., Biosens. Bioelectron. (2010), doi:10.1016/j.bios.2010.09.038

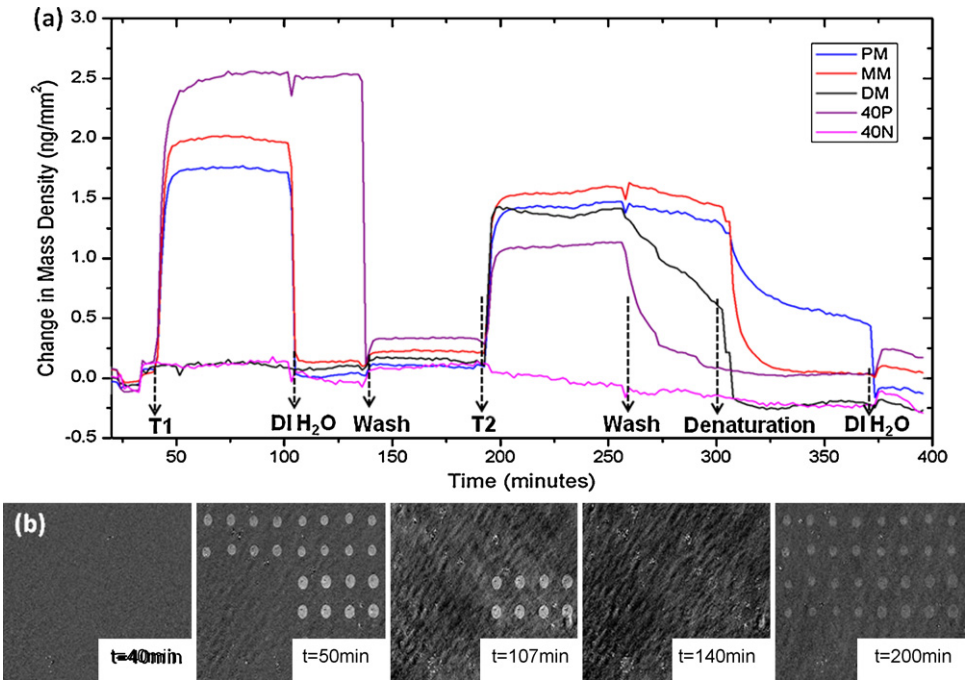

Fig. 4. DNA Hybridization: (a) 15 spots per probe type are averaged in the dynamic measurement. The mass density change is calculated by subtracting the average mass of the initial 20 min under the wash buffer prior to introducing the target. (b) The images of the array under different flow conditions are shown. The data from $t = 37$ min is subtracted as a reference. The images correspond to $t = 40$ min, 50 min, 107 min, 140 min, and 200 min, respectively.

α-HSA was flowed for 50 min and 2.6 ng/mm^2 mass increase was detected on the HSA spots while an additional 0.96 ng/mm^2 was detected on α-HSA spots where antigen had already been captured, creating a sandwich assay. RA was then flowed for 50 min and 0.7 ng/mm^2 of binding was detected on the α-RA spots. This was then followed by a 50 min flow of α-RA in which binding was detected on the RA and the α-RA showing 3.1 and 2 ng/mm^2 increases, respectively, once again showing the sandwich effect. Finally α-MA was flowed and 5.85 ng/mm^2 of binding was detected on the MA spots. At the end of the experiment 20 mM HCl was flowed to regenerate the initial probe surface. Targets where then flowed again and binding was observed with minimal degradation of the sensor surface.

Multiplexed detection of antigen–antibody interactions demonstrates the capability of the LED-IRIS platform to perform multiple tests on the same protein microarray and to potentially reuse the same microarray for repeated testing. While the protein experiment shown in Fig. 3 was conducted on an array of 60 spots, a microarray can be constructed from thousands of spots depending on the imaging sensor (CCD) area. Additionaly, for added confirmation in a diagnostic application, for example, a sandwich assay as demonstrated in the above experiment may be used to increase sensitivity by amplifying the signal. Likewise, in research applications, where understanding binding kinetics may be of interest, LED-IRIS is able to monitor dynamic binding interactions effectively.

3.3. Dynamic measurement of DNA hybridization and denaturation kinetics

The versatility of the LED-IRIS platform is demonstrated through monitoring of DNA hybridization and denaturation kinetics. Each of the five probes was spotted in a 4 × 2 array within a larger supergrid (Fig. 4a–s pot layout). The 40-mer sequences were used to show DNA hybridization and the 18-mer perfect match (PM), single mismatch (MM), and double mismatch (DM) sequences were used to study mismatch discrimination through denaturation kinetics. Two supergrids were monitored, and the average mass change of ~15 spots/probe is presented in Fig. 4a.

Before incubations, wash buffer was flowed for 30 min to remove any weakly bound DNA probes. After the initial wash buffer, 40-mer target (T1) was flowed for 60 min and hybridization with the 40-mer compliment probes (40P) was detected as indicated by 2.5 ng/mm^2 mass increase. Negative control probes (40 N) showed no change in mass. Note the weaker interaction of the T1 to the PM probes and MM probes as indicated by 2.0 ng/mm^2 and 1.6 ng/mm^2 mass increase respectively. No mass change was observed with DM probes. The relative mass increases between the different probes correlates well with the theoretical stability of the duplexes shown in supplementary material (Table S2). When wash buffer was introduced, partially hybridized duplexes formed by T1–PM and T1–MM were denatured immediately, where as no change was observed for the 40P probes. Deionized water was then flowed in for 1 hour to denature all duplexes and to remove any unbound oligonucleotides. Following the deionized water wash, 20-mer target (T2, a perfect complement to the PM probes with an additional nucleotide on each end) was introduced. All of the 18-mer probes – PM, MM and DM probes – showed mass increase of ~1.5 ng/mm^2. 40P probes showed weaker interactions with T2, hence the T2–40P duplex denatured immediately when the wash buffer was flowed.

To study mismatch discrimination, a buffer with much lower ionic strength (0.5 mM) was flowed in to denature duplexes with higher free energy. Noticeable denaturation occurred with 18DM probes under wash buffer, but denaturation of T2–PM and T2–MM duplexes was not observed until the denaturation buffer was flowed in. Denaturation of the T2–DM duplex was the fastest, and that of the T2–PM duplex was the slowest under the same buffer. To discriminate between the two different mutations from the perfect complimentary hybrids, the decay rates were found by fitting an exponential function of the form: $f = a_1 e^{-a_2 t} + a_3$ to the kinetic data acquired for each spot, where a_1, a_2 and a_3 are fitting parameters.

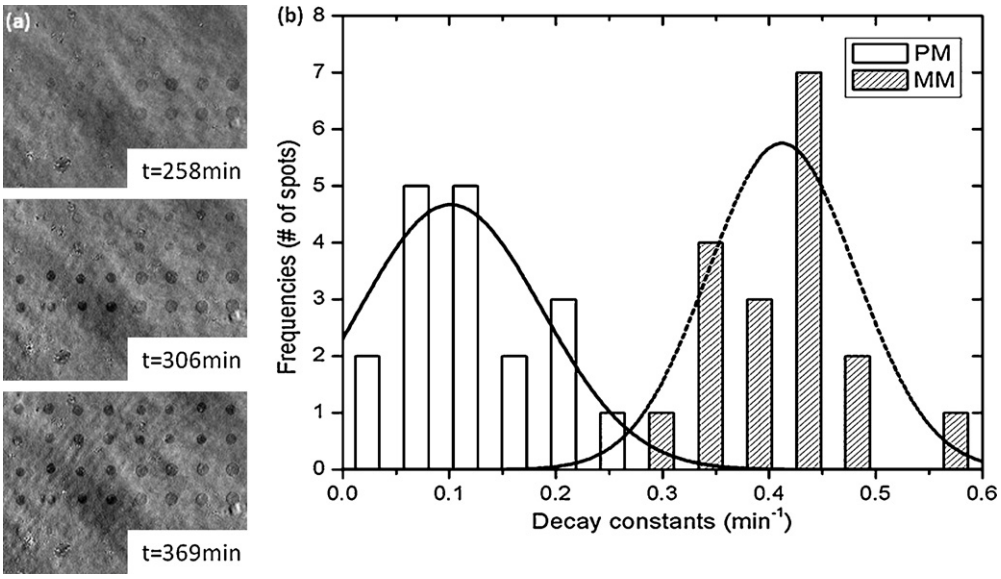

Fig. 5. DNA denaturing kinetics: (a) to show denaturation kinetics of different duplexes the images are subtracted by the data from $t = 300$ min as a reference. The images correspond to $t = 258$ min, 306 min, and 369 min, respectively. (b) Denaturation decay constants of T2–PM and T2–MM duplexes. Normal distribution is fitted with the shown histogram. The data from T2–DM duplex is not included as it is one order of magnitude higher.

Table 1
Decay constants for dehybridization of PM, MM, and DM.

	PM	MM	DM
Mean (1/min)	0.115	0.409	2.013
Standard deviation (1/min)	0.71	0.068	0.601
CL (%)	–	98.3	99.8

Although, a_1 and a_2 are not parameters of interest their inclusion in the fitting improves the quality of the fit because not all conditions start decaying from the same point. A histogram of the decay constants, a_2, for each probe is shown in Fig. 5b. A single mismatch in the hybrids shows a clear difference in the distribution of its decay rates. The confidence interval calculated for a single nucleotide mutation is 98.37% which is comparable to the mismatch discrimination ability shown by the IRIS with a laser illumination source (Özkumur et al., 2010). The confidence interval is calculated in the same way as was shown in the previous work. The decay constants of PM, MM, and DM probes are summarized in Table 1 along with the confidence interval for discriminating from the perfect complement. Finally, DI water was flowed in to complete denaturation of all DNA hybridized to immobilized probes.

4. Conclusion

We have demonstrated that our simple interferometric imaging technique using commercially available LEDs can achieve comparable sensitivity and throughput as the laser-based IRIS and SPRi systems such as the Biacore Instrument (GE Healthcare Life Sciences). Our technique is both label-free and quantitative, eliminating the need for fluorescent tagging and the use of secondary probes, while achieving high sensitivity and a wide linear dynamic range. We have demonstrated a dynamic in-solution measurement noise floor of 20 pm and a static dry measurement noise floor of 4 pm (Figure S1). Noise floors could further be reduced by increasing the spot area to average more pixels in the image or averaging more spots of the same probe. The LED-IRIS is capable of monitoring protein–protein binding interactions for antigen–antibody immunoassay applications as well as DNA binding interactions for base mismatch discrimination. We have demonstrated that the use of LEDs to conduct high-throughput biosensing imparts robustness without the loss of quantitative capabilities. Since low-cost commercially available LEDs are used, this technique allows for the potential development of compact, field deployable biosensors with no moving parts. The use of these LEDs also allows for the platform to be completely self-contained and operate at low power using batteries, thus eliminating the need for external power sources. Development of the LED-IRIS can fill the need for portable, reliable, and field-ready biosensors for both clinical and research applications where more complex and expensive systems cannot.

Acknowledgements

This work was partially funded by Army Research Laboratories (6) under the Contracts No. W911NF-06-2-0040, the Smart Lighting Engineering Research Center (EEC-0812056), and the MITRE Corporation under Research Agreement No.'s 79952, 80814, 81646. Approved for Public Release Case #10-2551. We also acknowledge Karishma Sekhon and Dr. Mario Cabodi for their assistance with the fluid flow chamber used in experiments.

Appendix A. Supplementary data

Supplementary data associated with this article can be found, in the online version, at doi:10.1016/j.bios.2010.09.038.

References

Andras, S., Adanyi, N., Szekacs, I., Majer-Baranyi, K., Istvan, S., 2009. Appl. Opt. 48 (4), B151–B158.
Cretich, M., Pirri, G., Damin, F., Solinas, I., Chiari, M., 2004. Anal. Biochem. 332 (1), 67–74.
Homola, J., Vaisocherova, H., Dostalek, J., Piliarik, M., 2005. Methods 37 (1), 26–36.
Lange, K., Herold, M., Scheideler, L., Geis-Gerstorfer, J., Wendel, H.P., Gauglitz, G., 2004. Dent. Mater. 20 (9), 814–822.
Lu, J.H., Strohsahl, C.M., Miller, B.L., Rothberg, L.J., 2004. Anal. Chem. 76 (15), 4416–4420.
MacBeath, G., Schreiber, S.L., 2000. Science 289 (5485), 1760–1763.
Mitchell, P., 2002. Nat. Biotechnol. 20 (3), 225–229.
Özkumur, E., Ahn, S., Yalcın, A., Lopez, C.A., Cevik, E., Irani, R.J., DeLisi, C., Chiari, M., Ünlü, M.S., 2010. Biosens. Bioelectron. 25 (1), 6.
Ozkumur, E., Needham, J.W., Bergstein, D.A., Gonzalez, R., Cabodi, M., Gershoni, J.M., Goldberg, B.B., Unlu, M.S., 2008. Proc. Natl. Acad. Sci. U.S.A. 105 (23), 7988–7992.

Ozkumur, E., Yalcin, A., Cretich, M., Lopez, C.A., Bergstein, D.A., Goldberg, B.B., Chiari, M., Unlu, M.S., 2009. Biosens. Bioelectron. 25 (1), 167–172.
Predki, P.F., 2004. Curr. Opin. Chem. Biol. 8 (1), 8–13.
Ramachandran, N., Larson, D.N., Stark, P.R.H., Hainsworth, E., LaBaer, J., 2005. Febs J. 272 (21), 5412–5425.
Ramsden, J.J., 1997. J. Mol. Recognit. 10 (3), 109–120.
Stears, R.L., Martinsky, T., Schena, M., 2003. Nat. Med. 9 (1), 140–145.
Vedula, R.S., Daaboul, G.G., Reddington, A., Ozkumur, E., Bergstein, D.A., Ünlü, M.S., 2010. J. Modern Opt., 1–6.
Winquist, F., Askendal, A., Elwing, H., 1997. Colloids Surf. B-Biointerf. 9 (1–2), 59–65.
Yeh, P., 1988. Optical Waves in a Layered Media. John Wiley & Sons, New York.
Yu, X.B., Xu, D.K., Cheng, Q., 2006. Proteomics 6 (20), 5493–5503.
Zhao, M., Wang, X.F., Nolte, D.D., 2008. Opt. Express 16 (10), 7102–7118.
Zhu, H., Bilgin, M., Bangham, R., Hall, D., Casamayor, A., Bertone, P., Lan, N., Jansen, R., Bidlingmaier, S., Houfek, T., Mitchell, T., Miller, P., Dean, R.A., Gerstein, M., Snyder, M., 2001. Science 293 (5537), 2101–2105.

Please cite this article in press as: Daaboul, G.G., et al., Biosens. Bioelectron. (2010), doi:10.1016/j.bios.2010.09.038